# Capillarity-Assisted Assembly of Carbon Nanotube Microstructures with Organized Initiations

**Xiaodai Lim,[†] Hee Wei Gary Foo,[‡] Guo Hao Chia,[‡] and Chorng-Haur Sow[†,*]**

[†]Department of Physics, Blk S12, Faculty of Science National University of Singapore 2 Science Drive 3, 117542 Singapore, and [‡]Dunman High School, 10 Tanjong Rhu Road, 436895 Singapore

**ABSTRACT** In this work, detailed studies of three different capillary-assisted techniques for the formations of large-scale multiwalled carbon-nanotube (MWNT)-based microstructures were presented. Using laser induced artificial vacancies, new insights into the effect of laser power, densities of MWNTs, and oxidation process dependencies for the creations of MWNT polygons were presented. With organized initiations, MWNT pillars were crafted out of MWNT arrays and 0.21 pL of water was found to produce sufficient force to bring about 14.7 μm deflections of a 9.19 × 9.19 × 24.1 $\mu m^3$ pillar, thereby allowing well-controlled formations of three-dimensional top-gathering MWNTs. Lastly, by twisting densified MWNT microbelts, 14 times improvements in resistivity as compared to undensified MWNT microwalls were achieved. Through prepatterning, the amount of twisting effect could be controlled, and this in turn allowed control of the resistance of the densified MWNT microwalls. These new insights and techniques presented could further encourage the use of self-organized MWNT structures with initiation as a flexible and viable route for the implementations of carbon-nanotube-based electronic devices.

**KEYWORDS:** carbon nanotubes · assembly · micropatterning · densification · water

Material fabrications are progressing into a phase where well-defined structures created using nanoscale materials becomes a key technology.[1] To facilitate such progress, self-assembly is an efficient and often preferred process to build micro- and nanomaterials into ordered macroscopic structures.[2] For example, Li *et al.*[3] utilized a self-assembly process to synthesize large-scale aligned carbon nanotube (CNT) honeycomb structures that exhibit superhydrophobic property. CNTs with their unique mechanical, electrical, and optical properties[4−7] are suitable for a wide variety of applications. As such, it is essential to be able to control the architecture of the CNTs on the substrates since such controlled assembly is crucial for applications in micromechanical actuators and composites.[8] Implementing an elegant water-assisted assembly process as reviewed by Liu *et al.*,[9] the structures at which the CNTs are defined can be divided into negative (CNTs are removed to form the pattern) and positive (where CNTs remained as the building block of the pattern) structures.

Chakrapani *et al.*[10] and Liu *et al.*[11] reported on the use of long-range capillary effect of water to assist the assembly of CNTs into desired negative structures. To do so, both groups introduced artificial vacant sites into as-grown vertically aligned CNT arrays. Once water was introduced to the system, it would be guided into the spaces between the CNTs. The resulting capillary action forces the water to reach and spread across the hydrophilic substrates (silicon/quartz), creating a hydrostatic dilation stress. The presence of the hydrostatic stress caused the CNTs to be flattened in the regions with lower CNT density, while allowing the CNTs to become tightly packed along the regions with higher CNT density.[11]

While both groups used similar water-assisted-assembly technique, different treatments were carried out on the CNT samples before the assembly process. During their sample preparation process, Chakrapani *et al.*[10] reported the use of pre-process technique of patterning the substrate on which the vertically aligned CNTs were synthesized to create the vacant sites. For the case of Liu *et al.*,[11] post synthesis treatment of using pulsed laser to pattern vacant sites on the CNTs was carried. With both work showing fixed amount of CNTs removed to create the vacancies, it would thus be interesting to determine the relationship between the eventual pattern formed from the CNTs and the amount of CNTs removed from the vacancies introduced. Moreover, due to the hydrophobic nature of the CNT surfaces, Chakrapani *et al.*[10] oxidized the patterned CNTs before the

*Address correspondence to physowch@nus.edu.sg.

Received for review September 11, 2009 and accepted December 28, 2009.

**Published online January 7, 2010.**
**10.1021/nn9012109**

introduction of water. However, in the case of Liu *et al.*[11] no oxidation of CNTs was mentioned. As such, it would be worthwhile to understand if oxidation of CNTs before and after the introduction of the vacancies would affect the resultant structures.

In the case of positive CNT structures, a method of prepatterning the substrate[10,12] was implemented. Wei *et al.*[12] reported on the ability to arrange CNTs in an organized manner through patterning $SiO_2$ on Si substrate. In doing so, they are able to produce simultaneous and multidirectional nanotube growth. Of the positive CNT structures reported, a random top gathering effect of the CNTs had been reported by Correa-Duarte *et al.*[13] These top gathering effect had also been observed in arrays of nanorods[14] as well as silicon nanolines[15] and photoresist polymer walls.[16,17] With well-defined 3D CNT structures having great potential as packing systems and CNT-based electronics, it would thus be useful to continue to develop techniques that facilitate the creations of well-controlled and large scale 3D CNT structures in a cost efficient manner.

In addition, with large-scale densification of shape defined 3D aligned CNT structures exhibiting improvements in conductivity,[18] such densification phenomena had opened up greater possibilities of incorporating CNTs in various applications such as flexible heater as well as supercapacitor electrodes for compact energy-storage devices.[18] In addition, flattening of aligned CNTs onto substrates also allowed applications of CNTs as microelectromechanical devices.[19] In addition, these flattened CNTs could be vertically suspended and stretched for use as sensing components.[20] With the vast amount of applications achievable from densified aligned CNTs, it would be of interest to determine if any twisting effect on the densified CNTs would result in better electrical conductivity.

In this report, three techniques involving capillary assisted-assembly of CNTs are presented. The first technique describes the creations of negative CNT structures *via* the use of water after artificial vacancies were patterned on the CNTs using focused laser beam pruning. These vacancies serve as initiation sites for the water-assisted assembly process. The effects of oxidization treatment on CNTs, density of CNTs, and laser power induced artificial vacancies on the assembly of CNTs were investigated. Studies of the formation process of the MWNT polygons were also conducted using quantum dots (QDs), and the results observed under fluorescence microscope (FM) were presented as Supporting Information (Figure S1). The second technique presents water-assisted large-scale assembly of top gathering pillar arrays made out of CNTs. This technique could possibly serve as an additional set of tools for further developments in controlling the architecture of the CNTs on the substrates for the creations of future CNT-based devices and packing systems. Lastly, a dip−dry method involving the use of ethanol to pack large-scale aligned and twisted CNT microbelts onto the substrate surfaces is introduced. This is followed by detailed *I*−*V* measurements of the respective type of packed CNT microbelts.

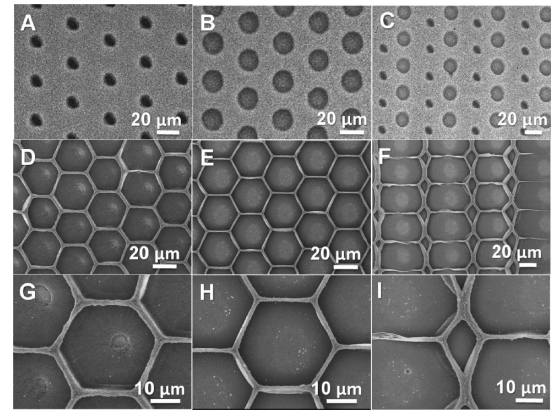


**Figure 1. SEM images of patterned vacant sites created using (A) 27 mW and (B) 50 mW and (C) a mixture of both laser power before water-assisted assembly. After water-assisted assembly, panels D and E show "walls" of the polygons forming approximately at the vertical bisector of two adjacent vacancies while panel F shows a shift in the positions of the polygon "walls". (G−I) Larger magnfications of the individual polygons formed in panels D−F.**

## RESULTS AND DISCUSSION

**Negative MWNT Microstructures.** ***Laser-Power-Dependent Study.*** Previous work by Liu *et al.*[11] reasoned the existence of a greater value of hydrostatic dilation stress in the regions with higher CNT density compared to that at the lower density. Owing to this difference, CNTs were flattened outward from a region of lower CNT density, while "walls" were formed when CNTs collapsing in opposite directions met. Thus, negative structures could be constructed through the introduction of artificial vacant sites with even lower density than those found naturally in the CNT arrays.

With that as the basis, effects of the depth and size of the vacant sites on the formation of the negative structures were investigated. A continuous focused laser beam[21] was used to create artificial vacant sites on vertically aligned multiwalled carbon nanotube (MWNT) arrays by releasing the laser intermediately with a shutter. Depths of the vacant sites were changed by varying the laser power from 50 to 27 mW. In doing so, the diameter of the laser induced vacancies changes from $13.0 \pm 0.2$ to $6.4 \pm 0.1$ μm with depth varying from 22.4 to 16.2 μm. A similar pattern of the vacant sites were created on same MWNT samples with Figure 1A showing the pattern formed using only 27 mW laser power while Figure 1B was created *via* 50 mW laser power. Figure 1C shows a mixture of sites created using 50 mW (larger holes) and 27 mW (smaller holes). After the completion of the initial vacancy patterning, the sample was exposed to the oxygen plasma to convert the surface into a hydrophilic one. Subsequently, distilled water was introduced to the oxidized patterned MWNT

surfaces and left to dry. Formations of the hexagonal structures shown in Figure 1D and Figure 1E were consistent with the proposed mechanism that the "wall" of the polygon would form approximately at the vertical bisector of two adjacent vacancies shown in Figure 1A and Figure 1B.[11] However, such phenomenon was only observed for vacancies created using the same laser power. With vacancies of different sizes (Figure 1C), the "wall" of the polygon was no longer positioned at the bisector of two adjacent vacancies created using different laser power as shown in Figure 1F.

A possible explanation could be as follows: because of the use of higher laser power, more MWNTs were removed from the surfaces as compared to those formed using lower laser power. Thereby creating an area of lower density (or larger vacancies) than those formed *via* lower laser power. Owing to such differences in density, the base of the smaller vacancies was mostly covered with bent MWNTs (Figure 1G), whereas the majority of the base from the larger vacancies shows more Si substrates (Figure 1H). Lower hydrostatic dilation stress existing in the larger vacancies, due interactions with the larger area of exposed Si substrate, would result in the MWNTs being drawn away readily from these sites. Hence, with a similar amount of water and evaporation time, the bending of MWNTs branching out from the center of the larger vacancies would occur over a larger distance. It was due to such variations in distance that shifted the positions of the polygon "wall" from the bisector of two adjacent vacancies (Figure 1I).

In addition to the shift in the positions of the polygon "walls", the polygon "walls" shown in Figure 1D were less compact as compared to those in Figure 1E. Such difference in the degree of packing of the polygon "walls" could also be attributed to the extent of the hydrostatic dilation stress experienced in both larger and smaller vacancies. With the distance between two larger vacancies being the same that those between two smaller vacancies, lower hydrostatic dilation stress experienced in the larger vacancies would cause the MWNTs making up the polygon "walls" to be more compacted as compared to those between the smaller vacancies.

Although Liu *et al.*[11] had conducted studies regarding how the height of the CNT and the distance between the vacancies could affect the eventual formations of the polygons; no studies regarding the dependencies of the formation of the polygons on laser power had been reported thus far. Hence the work presented could provide an alternative way to create polygons of different structures.

***Density-Dependent Study.*** Previous work by both Chakrapani *et al.*[10] and Liu *et al.*[11] suggested that the formations of polygons could be a resultant of different CNT densities on the array, and they further verified their proposal with vacancy-initiated polygon formations. However, no detailed studies had yet to be presented

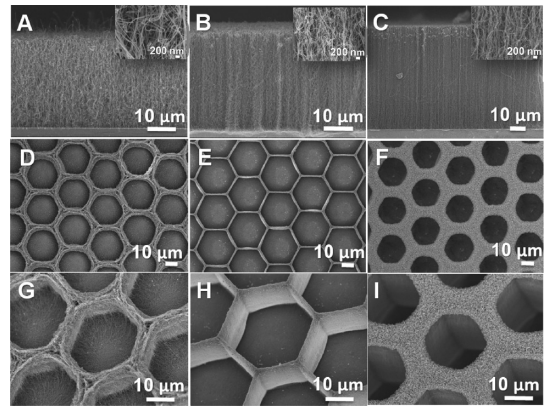


**Figure 2. SEM images of vacant sites created using 50 mW laser power on MWNTs with different density: (A) 0.95 × $10^9$ MWNT $cm^{-2}$; (B) 1.87 × $10^9$ MWNT $cm^{-2}$ and (C) 2.92 × $10^9$ MWNT $cm^{-2}$. (Insets show higher magnifications of the MWNTs.) The respective polygons form on the MWNTs after interaction with water was as shown in panels D−F. (G−I) Higher magnifications of individual polygons taken at an angle of 25.0°.**

regarding how the densities of different CNT arrays could affect the polygons formed, given the same design of vacancies created on the arrays. Thus to investigate the effect of the density of MWNTs on the formations of these polygons, a similar vacancy pattern shown in Figure 1B was created on MWNTs using 50 mW laser power with MWNT density ranging from 0.95 × $10^9$ MWNT $cm^{-2}$ (Figure 2A), 1.87 × $10^9$ MWNT $cm^{-2}$ (Figure 2B), and 2.92 × $10^9$ MWNT $cm^{-2}$ (Figure 2C). After the oxidation treatment, the respective polygons formed following the water-assisted assembly are shown in Figure 2(D−F) with Figure 2(G−I) showing higher magnification of the corresponding individual polygon. From the MWNTs with the lowest density (Figure 2(D, G)), small cracks were observed to form in between the polygon "walls" due to presence of many natural regions with low MWNT density. In the case of MWNTs with higher density (Figure 2(F, I)), limitations to the packing of the polygon "walls" were observed. In the process of the formation of the polygons, larger force was required to bend the densely packed MWNTs (Figure 2C) as compared to the loosely packed MWNTs in Figure 2A. Given the same amount of water, hence similar time restriction, there was insufficient time for the polygons to form. Moreover, unlike the sample shown in (Figure 2H), no smaller cracks were observed to form in the polygon walls of Figure 2(F, I) as the artificial sites produce much lower density than those found naturally on the MWNT sample. On the basis of the results, an ideal density for the formation of polygons would be expected to exist between 0.95 × $10^9$ MWNT $cm^{-2}$ (Figure 2G) and 2.92 × $10^9$ MWNT $cm^{-2}$ (Figure 2I). Using MWNTs with density of 1.87 × $10^9$ MWNT $cm^{-2}$ (Figure 2B), polygons with well-packed walls were obtained (Figure 2H).

***Oxidation-Dependent Study.*** On the basis of our previous studies, we determined that exposure to oxygen

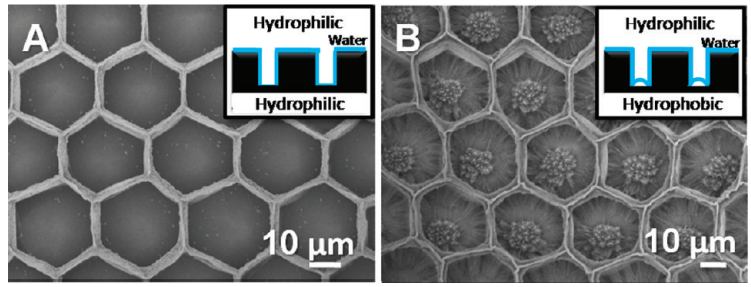


**Figure 3. SEM images of capillary-assisted MWNT patterns on samples with vacant sites created using focused laser (50mW) on MWNTs with (A) prior oxidation and (B) postoxidation. Insets show proposed mechanisms for the formations of different types of MWNTs polygons.**

plasma readily converts hydrophobic MWNTs into hydrophilic ones. Using laser trimming to remove the top layer of the oxidized MWNTs, the hydrophilic surface would revert to being hydrophobic.[22] Hence by changing the sequence of oxidation after (Figure 3A) and before (Figure 3B) the creation of artificial vacant sites, different types of capillary-assisted polygons were formed. From Figure 3A, polygons with the base covered with flattened MWNTs were observed as compared to the aggregations of MWNTs at the center of the polygons for MWNTs with vacancies created after oxidation (Figure 3B). When vacancies were created prior to oxidation, oxygen ions would be able to functionalize the interior of the vacancies as well, thereby allowing the smooth flowing of water into the vacancies as illustrated in the inset of Figure 3A. Reversing the process, the vacancies created after oxidation would reveal MWNTs that revert back to their hydrophobic nature.[22] With a hydrophilic top surface, water was able to spread across the MWNT surface. Assisted by gravity, water was able to sip into the vacancies. However, at the base of the vacancies, formations of air pockets due to hydrophobic nature of the MWNTs hindered the creation of a hydrostatic dilation stress as no interactions between the water and the substrate could occur at the center of the vacancies. Hence clustering of MWNTs at the center of the vacancies would occur together with packing of MWNTs along the polygon "walls".

**Effect of Capillarity Forces on the Formations of Microstructures under Fluorescence Microscope.** With the above studies as well as those previously reported by Chakrapani *et al.*[10] and Liu *et al.*[11] being conducted with the samples kept in an upright position while the polygons were formed, both gravitational and capillarity effects would occur in the opposite direction to the normal of the MWNT surface. Hence, allowing the formations of hydrostatic dilation stress due to interactions between water and the MWNT substrates. As such, a study of how the competition between gravitational and capillarity effect could affect the formations of these MWNT polygons could provide further insights to the reasons behind the formation of the polygons. Experiments were conducted using quantum dots (QDs) suspensions and the formation process of the MWNT polygons were observed under fluorescence microscope (FM). Due to differences in the duration and the amount of QDs mixture that filled up the vacant sites, well-defined MWNT polygons with different types of bases were formed. These structures thus allow possible applications as seeding sites for tissue culture.[13] Detailed results and discussion of the experiments could be found in the Supporting Information section.

**Positive MWNT Microstructures.** Making use of the competition between gravitational and capillary forces, together with a controlled amount of water, one could restrict the clustering of MWNTs to the surface of the MWNTs. Together with the use of focused laser beam, water-assisted top gathering MWNT pillars could be created. Although the top gathering effect of photoresist[14,16] and silicon nanostructures,[14,15] together with the random top gathering effect of CNT arrays,[13,23] had been achieved, to the best of our knowledge, there has yet to be any report on the controlled top gathering effect of CNT pillars.

**Technique for the Formation of Positive MWNT Microstructures.** With hydrostatic stress being identified as the driving force behind the collapse of MWNTs from regions of lower densities toward that of higher densities,[11] one could create a wide variety of microstructures that bend toward each other. Examples of such structures include pillars of MWNTs. By maintaining large distances between each cluster of MWNT pillars, empty spaces could be created between each cluster. Consequently, water induced hydrostatic stress would cause the pillars to bend toward each other, thereby creating top gathering MWNTs.

MWNT pillars in groups of three or four, were crafted out of as-grown MWNTs (Figure 4A) using a focused laser beam (Figure 4B). The patterned MWNTs were oxidized using reactive ion etching (RIE) and placed inversely onto the surface of distilled water (Figure 4C). In doing so, when the sample is removed from the water surface, the minima volume of water required to wet the MWNTs completely would remain on the MWNTs (Figure 4D). As the water evaporates while maintaining the samples in an inverted manner, capillary-assisted top gathering of the MWNT pillars were formed. (Figure 4E).

**Water-Assisted Assembly of Positive MWNT Microstructures.** On the basis of the above technique, an ordered array of MWNT pillars as illustrated in the inset of Figure 5A, was found to collapse in a random manner. However, with pillars created in clusters of four pillars separated by large spacing (Figure 5B, inset), the MWNTs were found to gather at the top in an orderly manner. The results shown in Figure 5(A,B) thus verified the above proposed technique for the formation of top-gathering MWNT pillars. Rearranging the positions of the pillars as shown in the inset of Figure 5C, the three-pillar clusters were observed to gather at the top-portion of the pillars within the clusters. Tilted views (40°) of the top-gathering MWNT pillars were as shown in Figure 5(D,E). From both images, MWNT pillars were observed to gather at the top regions with the base of the MWNT pillars remaining attached to the Si substrate. As such, through creations of both high and low density regions in the MWNT array, one could easily control the eventual formations of the top-gathering MWNTs.

**Analysis of Top-Gathering MWNTs.** For the analysis of the top-gathering MWNT pillars, a beam sway model, similar to the one proposed by Deguchi *et al.*[24] to calculate the maximum resist deflection in synchrotron radiation lithography, was used. An individual MWNT pillar was treated as a beam supported at one end as shown in Figure 6. In this case, the relation between the Young's modulus and the maximum deflection is expressed by

$$E = \frac{\gamma_w H^4}{8I}\left(\frac{1}{\delta_{max}}\right) \quad (1)$$

where $E$ is the Young's modulus, $\gamma_w$ is the surface tension of water, $H$ is the pillar height, $\delta_{max}$ is maximum deflection, and $I$ is the second moment of area expressed by

$$I = \frac{1}{12}DL^3 \quad (2)$$

Here $L$ is the width of the pillar and $D$ is the breadth of the pillar. Substituting eq 2 into eq 1, the Young's modulus of the MWNT pillar can be expressed as

$$E = 1.5HA^3\left(\frac{\gamma_w}{D}\right)\left(\frac{1}{\delta_{max}}\right) \quad (3)$$

where $A$ is the aspect ratio ($H/L$). As such, the Young's modulus of the MWNT pillar, $E$, hence the pillar's flexural stiffness (EI), is proportional to the height, $H$ of the MWNTs as well as the third power of the aspect ratio, $A$, of the MWNT pillar. It is also inversely proportional to the maximum deflection, $\delta_{max}$ experienced by the pillar.

Considering a cluster of four MWNT pillars as shown in Figure 7, with the MWNT pillars gathering at the center of the cluster, the maximum deflection that the pillars could undergo in this configuration was found to be 22.6 μm. Substituting this value into eq 3, and with the other variables obtained from Figure 7, the estimated Young's modulus of the MWNT pillars was found to be ~11.9 MPa. With the surface tension of water[11] as 72.8 mN $m^{-1}$ and the height $H$ of the MWNTs found to be ~ 20.8 μm, a force of ~1.98 μN would be sufficient to bring about such a top-gathering effect of the MWNT pillars.

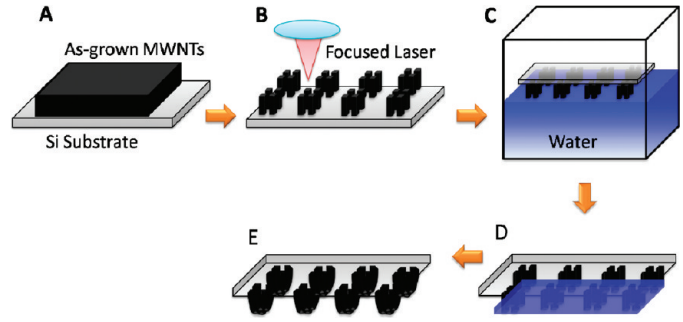


**Figure 4. Schematic of the procedure to create positive MWNT microstructures: (A) as-grown MWNT array; (B) creating MWNT pillars using focused laser beam; (C) inverting MWNT pillars over water; (D) keeping the samples inverted while drying; and (E) formations of top gathering MWNT pillars.**

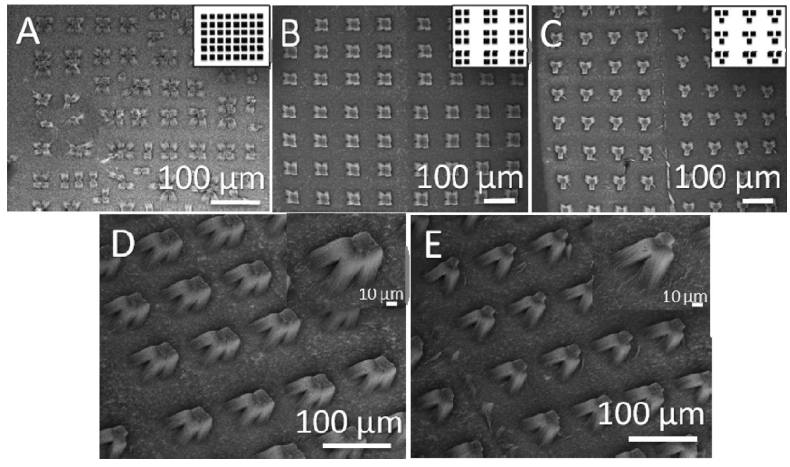


**Figure 5. SEM images of capillary-assisted (A) randomly collapsed MWNT pillars; ordered top-gathering of (B) four and (C) three MWNT pillars. Insets A−C are schematics showing the respective positions of the MWNT pillars before water-assisted assembly. (D,E) SEM images taken at a 40° tilt of the top-gathering (D) four and (E) three MWNT pillars. Insets D and E are higher magnifications of the respective clusters of MWNT pillars.**

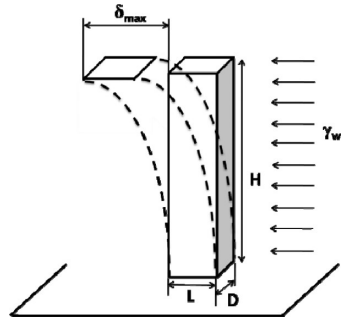


**Figure 6. Illustration of the beam sway model used in the analysis of the top-gathering MWNT pillars.**

However, it should be noted that such top-gathering phenomenon of the MWNT pillars could be separated into micro- and nanoscale. In the beam sway model proposed, only the microscopic effects were considered. With MWNT pillars being made up of ~4000 individual MWNTs, capillary forces acting on the individual MWNTs as water evaporates from the MWNT surface also had to be taken into consideration for such phenomenon to occur.

*In situ* observations of such capillary-induced top-gathering MWNT pillars could be observed using a side-view optical microscope. As shown in the series of snapshots (Figure 8(A−E)) while the water droplet which lands on two MWNT pillars evaporates, the MWNT pillars were found to gather at the top. SEM images of the gathered MWNT pillars taken from top view showed that capillary forces resulting from the evaporation of a water droplet with volume of ~0.21 pL is sufficient to induce a deflection of a MWNT pillar with dimensions 9.2 μm (*L*) × 9.2 μm (*D*) × 24.1 μm (*H*), over a distance of 14.7 μm.

**Large-Scale Collapsing of MWNT Microwalls by Dip−Dry Method.** In addition to the ability to create both positive and negative structures into desired configurations and at specific positions, large-scale MWNT microwalls could be collapsed *via* a dip−dry method to form MWNT microbelts. To do so, parallel MWNT microwalls were crafted out of as-grown MWNTs on quartz *via* a focused laser beam as shown in Figure 9(A,B). The laser pruned MWNTs were then submerged into a small amount of ethanol reservoir and pulled vertically out of the wetting agent as illustrated in Figure 9C. The extracted MWNT samples were left to dry vertically and the dried sample comprised MWNT microbelts as shown in Figure 9D.

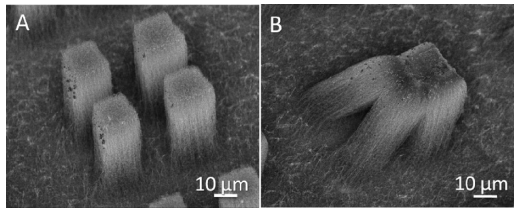


**Figure 7. SEM images taken at 40° tilt, showing four MWNT pillars: (A) before and (B) after water-assisted top-gathering.**

MWNT microwalls as long as 4 mm with a width of 10 μm were pruned from the MWNT array. The images could be found under Figure S2A and Figure S2B of the Supporting Information. Upon collapsing the MWNT microwalls to form MWNT microbelts, two probe *I*−*V* measurements were conducted on the collapsed MWNT microbelts using probe tips of diameter 2.4 μm. From the results shown in Figure S2G, the average total resistance of the MWNT microwalls before collapsing was ~70 kΩ, whereas that of the MWNT microbelts was ~20 kΩ. Thus by simply undergoing the dip−dry method of packing the MWNTs to the substrate, an approximately 3.5-fold reduction in resistivity and a corresponding 3.5-fold improvement in current measured from the MWNT microbelts were achieved. Such improvements were consistent with those reported by Futaba *et al.*[18] and Hayamizu *et al.*[19]

In addition to the *I*−*V* measurements conducted across fully collapsed MWNT microbelts, similar measurements were also conducted at different positions of the MWNT microbelts. These include measurements along the length of the MWNTs that made up the walls, across twisted MWNT microbelts and across MWNT microbelts that had collapsed together. For these measurements, five to six sets of readings were taken for each point of measurements, and the average values were obtained. The average values of the *I*−*V* measurements plotted in Figure 10A were obtained from configurations B, C, and D as shown in the corresponding optical images in Figure 10(B−D). *I*−*V* measurements taken of the quartz substrate on which the samples were prepared, as well as measurements of the microwalls before and after collapsing into microbelts, were also presented in Figure 10A. By changing the position of the two probe tips from across the length of the collapsed microbelt to along the length of the MWNTs that made up the microwall (Figure 10B), a change in resistance from ~20 to ~11 kΩ was achieved. A resistivity of ~6 kΩ was obtained when measurements were made across two MWNT walls that had collapsed toward each other. The least amount of resistivity was achieved when measurements were taken across a twisted MWNT channel. From such a structure, a resistivity of ~5 kΩ was detected.

Based on above experiments, by simply twisting the MWNT microwalls by 180°, a reduction in resistivity by as much as 14 times, as compared to the MWNT microwalls before collapsing, could be achieved. As such, to achieve greater control over the twisting effect of the MWNT walls, laser pruning was used to pattern the MWNT array into the wavy structures shown in Figure 11(A, C). Junctions between the parallel walls were designed to possess an angle of 45° (Figure 11A) and 90° (Figure 11C). Using the assembly method illustrated in Figure 9, the assembled MWNT microbelts were as shown in the optical images of Figure 11(B, D). Comparing the regions boxed out in Figure 11(B, D), different

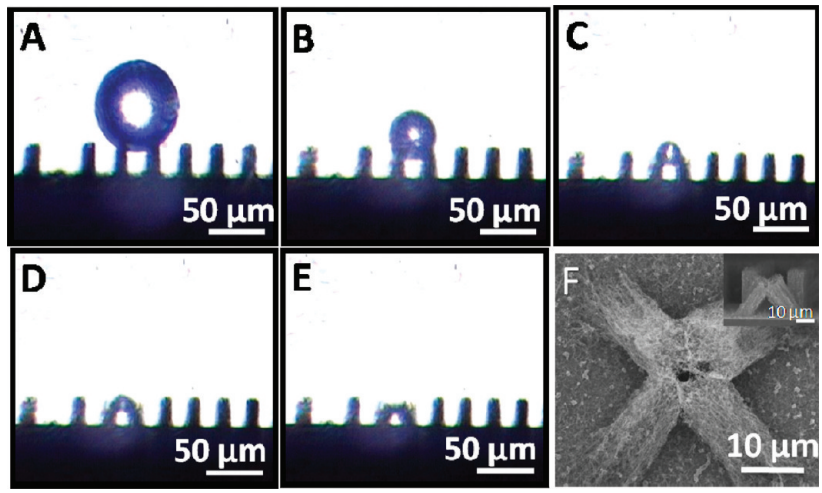


**Figure 8. (A−E) Optical images of capillarity-assisted top-gathering of MWNT pillars as the water droplet evaporates. (F) SEM image showing the top view of the gathered pillars. (Inset of panel F is the side view of the same set of top-gathering pillars.)**

types of twisting to the MWNT walls could be observed by simply changing the angle at which the walls were joined. From both Figure 11B and Figure 11D, the MWNT microwalls were twisted at an angle similar to that predetermined by the laser prune structures. As such, it could be verified that through laser pruning and using the dip-dry method of assembling MWNT microwalls, the degree at which the MWNT walls were twisted could be varied. In turn, the resistance of the packed-downed MWNT walls could be controlled.

## CONCLUSION

In conclusion, three different capillarity-assisted assemblies of both positive and negative MWNT microstructures were presented. Using the first method of introducing artificial vacancies, laser power, densities of

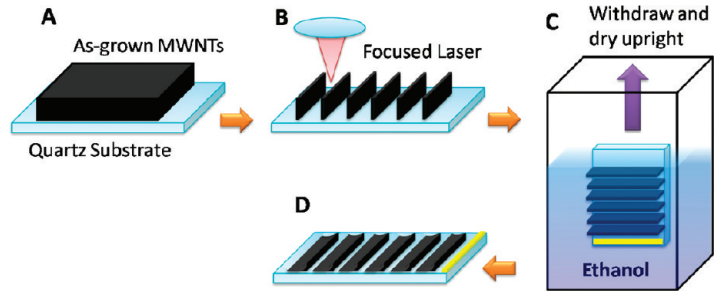


**Figure 9. Schematic of the dip−dry method used in collapsing large-scale MWNT microwalls: (A) as-grown MWNT arrays; (B) focused laser beam was used to create MWNT microwalls; (C) the patterned MWNT sample was placed into a container of ethanol and withdrawn vertically; and (D) the MWNT microwalls collapsed into MWNT microbelts. The yellow bar indicates the direction in which the sample was removed from the ethanol.**

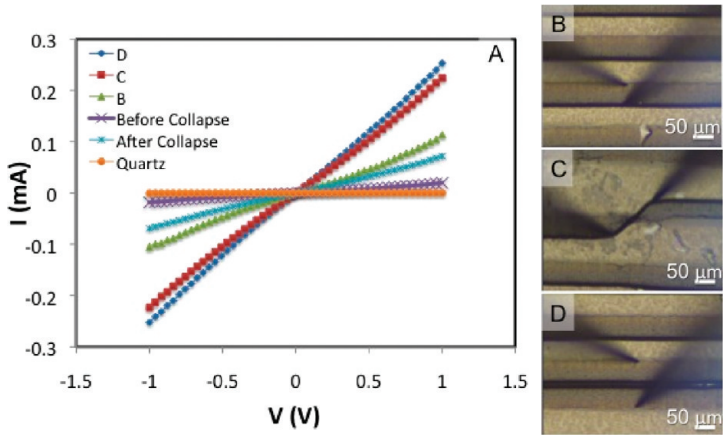


**Figure 10. (A) *I*−*V* measurements of the MWNT microwalls before and after collapsing into microbelts. The *I*−*V* curves indicated as B, C, and D corresponded to the *I*−*V* measurements taken at the respective positions of the microbelts as shown in the optical images on the right (indicated as B, C, and D).**

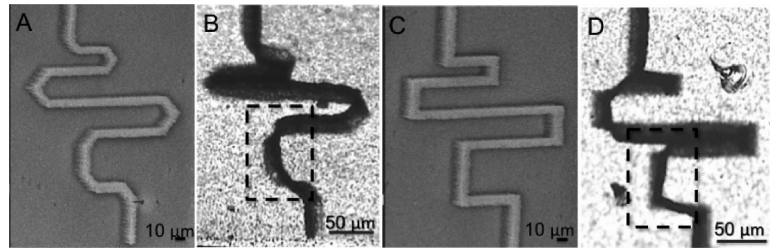


**Figure 11. (A, C) SEM images of different curve structures created *via* laser pruning on MWNT arrays. (B, D) Ethanol assisted assembly of twisted MWNT walls. The dotted rectangle box outlined similar regions on both structures except for the angle at which the parrallel MWNT walls were joint.**

MWNTs, and oxidation process dependencies for the creations of negative MWNT microstructures were investigated. With the results showing that *via* the use of different laser power, the polygon "walls" were observed to shift from the vertical bisector between two adjacent artificial vacancies. Proposed ideal density of well-formed MWNT polygons was determined to be between $0.95 \times 10^9$ MWNT $cm^{-2}$ and $2.04 \times 10^9$ MWNT $cm^{-2}$ and the importance of the sequence in which the MWNT samples were oxidized was presented. Positive microstructures made up of top gathering MWNT pillars were created and 0.21 pL of water was found to produce sufficient force to bring about 14.7 μm deflections of a $9.19 \times 9.19 \times 24.1$ $\mu m^3$ pillar. Lastly, using a dip−dry method, densification of large scale MWNT microwalls was achieved. By twisting densified MWNT microbelts, resistivity of the microbelts was found to improve by 14 times as compared to undensified MWNT microwalls. Through prepatterning, the amount of twisting effect on the densified MWNT microwalls could be controlled and this in turn could allow control of the resistance of the densified MWNT microwalls.

## METHODS

**Growth of MWNTs.** Aligned multiwalled carbon nanotubes (MWNTs) with typical length of 40−60 μm were grown on clean N-typed silicon (5 mm × 5 mm, Si (100)) substrates containing native oxide layer or quartz (4 mm × 4 mm) substrates. Before growth, a layer of iron film was coated on the substrates as catalyst using a magnetron sputtering system (model: RF Magnetron Denton Discovery 18). The coating rate was 4 nm $min^{-1}$ lasting for 6 min. These MWNTs were synthesized using a plasma enhanced chemical vapor deposition (PECVD) system, and details of the growth process were reported elsewhere.[25]

**Laser Pruning.** A laser pruning technique[21] involving a focused continuous laser beam of wavelength 660 nm with 3 mm initial beam diameter and a computer controlled sample stage was used to create arrays of artificial vacant sites on the MWNT surfaces. By focusing the laser beam using an optical lens, the beam size can be reduced. Setting the laser power to 50 and 27 mW, vacant sites of different sizes and depths were produced on the same MWNT array at specific locations. Using 50 mW focused laser beam, pillars in clusters of three and four, of specific dimensions located in the desired orientation, and the MWNT microwalls were controllably pruned out of the MWNT array.

**Oxidation of MWNTs.** Both pre- and postpatterned MWNTs were oxidized using a SAMCO RIE-10N reactive ion etching unit at a base pressure of $4 \times 10^{-6}$ Torr. MWNTs were placed on a RF-driven capacitatively coupled electrode. RF power was set at 20 W with 1 W reflected power. Work pressure was 0.05 Torr in the chamber and temperature was kept at 20 °C. During the RIE process, the flow rate of oxygen was set at 34.50 sccm (standard cubic centimeter per minute) with fixed durations of 30 s.

**Electrical Measurements.** The electrical measurements were carried out using a microprobe station (CascadeTM Microtech) equipped with an optical microscope to aid direct visualization. Probe tips of diameter 2.4 μm were used to conduct all current−voltage measurements. Voltage was measured *via* the Keithley 6430 source meter under current bias.

**Further Characterizations.** Further characterizations of the samples were carried out using field emission scanning electron microscope (FESEM, JEOL JSM-6400F) and fluorescence microscope (FM, Olympus IX71S1F-3 Inverted Microscope).

*Acknowledgment.* The authors acknowledge the funding support of MOE-ARF Grant R-144-000-211-112.

*Supporting Information Available:* Results obtained from the study of the effect of capillary forces on the formations of microstructures under fluorescence microscope as well as *I*−*V* measurements of collapsed MWNT microbelts; real time video capture of the formation process of the MWNT polygons. This material is available free of charge *via* the Internet at http://pubs.acs.org.

## REFERENCES AND NOTES

1. Nishikawa, T.; Nishida, J.; Ookura, R.; Nishimura, S. I.; Wada, S.; Karino, T.; Shimomura, M. Mesoscopic Patterning of Cell Adhesive Substrates as Novel Biofunctional Interfaces. *Mater. Sci. Eng. C* **1999**, *10*, 141–146.
2. Shimoda, H.; Oh, S. J.; Geng, H. Z.; Walker, R. J.; Zhang, X. B.; McNeil, L. E.; Zhou, O. Self-Assembly of Carbon Nanotubes. *Adv. Mater.* **2002**, *14*, 899–901.
3. Li, S. H.; Li, H. J.; Wang, X. B.; Song, Y. L.; Liu, Y. Q.; Jiang, L.; Zhu, D. B. Super-Hydrophobicity of Large-Area Honeycomb-like Aligned Carbon Nanotubes. *J. Phys. Chem. B* **2002**, *106*, 9274–9276.
4. Wildoer, J. W. G.; Venema, L. C.; Rinzler, A. G.; Smalley, R. E.; Dekker, C. Electronic Structure of Atomically Resolved Carbon Nanotubes. *Nature* **1998**, *391*, 59–62.
5. Treacy, M. M. J.; Ebbesen, T. W.; Gibson, J. M. Exceptionally High Young's Modulus Observed for Individual Carbon Nanotubes. *Nature* **1996**, *381*, 678–680.
6. Jang, J. W.; Lee, D. K.; Lee, C. E.; Lee, T. J.; Lee, C. J.; Noh, S. J. Metallic Conductivity in Bamboo-Shaped Multiwalled Carbon Nanotubes. *Solid State Commun.* **2002**, *122*, 619–622.
7. Tekleab, D.; Czerw, R.; Carroll, D. L.; Ajayan, P. M. Electronic Structure of Kinked Multiwalled Carbon Nanotubes. *Appl. Phys. Lett.* **2000**, *76*, 3594–3596.
8. Baughman, R. H.; Zakhidov, A. A.; de Heer, W. A. Carbon Nanotubes—The Route toward Applications. *Science* **2002**, *297*, 787–792.
9. Liu, H.; Zhai, J.; Jiang, L. Wetting and Anti-wetting on Aligned Carbon Nanotube Films. *Soft Matter* **2006**, *2*, 811–821.

10. Chakrapani, N.; Wei, B. Q.; Carrillo, A.; Ajayan, P. M.; Kane, R. S. Capillarity-Driven Assembly of Two-Dimensional Cellular Carbon Nanotube Foams. *Proc. Natl. Acad. Sci. U.S.A.* **2004**, *101*, 4009–4012.
11. Liu, H.; Li, S. H.; Zhai, J.; Li, H. J.; Zheng, Q. S.; Jiang, L.; Zhu, D. B. Self-Assembly of Large-Scale Micropatterns on Aligned Carbon Nanotube Films. *Angew. Chem., Int. Ed.* **2004**, *43*, 1146–1149.
12. Wei, B. Q.; Vajtai, R.; Jung, Y.; Ward, J.; Zhang, R.; Ramanath, G.; Ajayan, P. M. Organized Assembly of Carbon Nanotubes—Cunning Refinements Help to Customize the Architecture of Nanotube Structures. *Nature* **2002**, *416*, 495–496.
13. Correa-Duarte, M. A.; Wagner, N.; Rojas-Chapana, J.; Morsczeck, C.; Thie, M.; Giersig, M. Fabrication and Biocompatibility of Carbon Nanotube-Based 3D Networks as Scaffolds for Cell Seeding and Growth. *Nano Lett.* **2004**, *4*, 2233–2236.
14. Fan, J. G.; Dyer, D.; Zhang, G.; Zhao, Y. P. Nanocarpet Effect: Pattern Formation During the Wetting of Vertically Aligned Nanorod Arrays. *Nano Lett.* **2004**, *4*, 2133–2138.
15. Namatsu, H.; Kurihara, K.; Nagase, M.; Iwadate, K.; Murase, K. Dimensional Limitations of Silicon Nanolines Resulting from Pattern Distortion due to Surface Tension of Rinse Water. *Appl. Phys. Lett.* **1995**, *66*, 2655–2657.
16. Ye, J.; Matthews, M. A.; Darvin, C. H. Prevention of Photoresist Pattern Collapse by Using Liquid Carbon Dioxide. *Ind. Eng. Chem. Res.* **2001**, *40*, 5858–5860.
17. Tanaka, T.; Morigami, M.; Atoda, N. Mechanism of Resist Pattern Collapse During Development Process. *Jpn. J. Appl. Phys., Part 1* **1993**, *32*, 6059–6064.
18. Futaba, D. N.; Hata, K.; Yamada, T.; Hiraoka, T.; Hayamizu, Y.; Kakudate, Y.; Tanaike, O.; Hatori, H.; Yumura, M.; Iijima, S. Shape-Engineerable and Highly Densely Packed Single-Walled Carbon Nanotubes and Their Application as Super-Capacitor Electrodes. *Nat. Mater.* **2006**, *5*, 987–994.
19. Hayamizu, Y.; Yamada, T.; Mizuno, K.; Davis, R. C.; Futaba, D. N.; Yumura, M.; Hata, K. Integrated Three-Dimensional Microelectromechanical Devices from Processable Carbon Nanotube Wafers. *Nat. Nanotechnol.* **2008**, *3*, 289–294.
20. Lee, B. Y.; Heo, K.; Bak, J. H.; Cho, S. U.; Moon, S.; Park, Y. D.; Hong, S. Scalable Assembly Method of Vertically-Suspended and Stretched Carbon Nanotube Network Devices for Nanoscale Electro-Mechanical Sensing Components. *Nano Lett.* **2008**, *8*, 4483–4487.
21. Lim, K. Y.; Sow, C. H.; Lin, J. Y.; Cheong, F. C.; Shen, Z. X.; Thong, J. T. L.; Chin, K. C.; Wee, A. T. S. Laser Pruning of Carbon Nanotubes as a Route to Static and Movable Structures. *Adv. Mater.* **2003**, *15*, 300–303.
22. Li, P. H.; Lim, X. D.; Zhu, Y. W.; Yu, T.; Ong, C. K.; Shen, Z. X.; Wee, A. T. S.; Sow, C. H. Tailoring Wettability Change on Aligned and Patterned Carbon Nanotube Films for Selective Assembly. *J. Phy. Chem. B* **2007**, *111*, 1672–1678.
23. Lee, S. H.; Lin, C. H.; Chiou, J.-M.; Kuo, C. T. Effects of Post Treatment on the Field Emission Properties of CNTs Grown by ECR-CVD. *Diamond Relat. Mater.* **2006**, *15*, 854–858.
24. Deguchi, K.; Miyoshi, K.; Ishii, T.; Matsuda, T. Patterning Characteristics of a Chemically-Amplified Negative Resist in Synchrotron Radiation Lithography. *Jpn. J. Appl. Phys., Part 1* **1992**, *31*, 2954–2958.
25. Wang, Y. H.; Lin, J.; Huan, C. H. A.; Chen, G. S. Synthesis of Large Area Aligned Carbon Nanotube Arrays from $C_2H_2-H_2$ Mixture by Rf Plasma-Enhanced Chemical Vapor Deposition. *Appl. Phys. Lett.* **2001**, *79*, 680–682.